Mesoporous Biocompatible and Acid-Degradable Magnetic Colloidal Nanocrystal Clusters with Sustainable Stability and High Hydrophobic Drug Loading Capacity

Bin Luo,[†] Shuai Xu,[†] An Luo,[‡] Wen-Rui Wang,[§] Shi-Long Wang,[§] Jia Guo,[†] Yao Lin,[⊥] Dong-Yuan Zhao,[∥] and Chang-Chun Wang[†,*]

[†]Key Laboratory of Molecular Engineering of Polymers (Minister of Education), Department of Macromolecular Science, and Laboratory of Advanced Materials, Fudan University, Shanghai 200433, People's Republic of China, [‡]School of Chemical and Environmental Engineering, Shanghai Institute of Technology, Shanghai 200433, People's Republic of China, [§]Shanghai Key Laboratory of Cell Signaling and Diseases and School of Life Science and Technology, Tongji University, Shanghai 200092, People's Republic of China, [⊥]Polymer Program, Institute of Materials Science & Department of Chemistry, University of Connecticut, Storrs, Connecticut 06269, United States, and [∥]Department of Chemistry, and Laboratory of Advanced Materials, Fudan University, Shanghai 200433, People's Republic of China

ABSTRACT Fabrication of magnetic particles (MPs) with high magnetization and large surface area simultaneously is critical for the application of MPs in bioseparation and drug delivery but remains a challenge. In this article, we describe an unprecedented approach to synthesize mesoporous magnetic colloidal nanocrystal clusters (MCNCs) stabilized by poly(γ-glutamic acid) (PGA) with high magnetization, large surface area (136 m^2/g) and pore volume (0.57 cm^3/g), excellent colloidal stability, prominent biocompatibility, and acid degradability. This result provides the important step toward the construction of a new family of MCNCs and demonstrates its capacity in a "magnetic motor" drug delivery system. Here, as an example, we explore the applicability of as-prepared mesoporous MCNCs as hydrophobic drug delivery vehicles (paclitaxel as model drug), and the resultant loading capacity is as high as 35.0 wt %. The antitumor efficacy measured by MTT assay is significantly enhanced, compared with free drugs. Thus, combined with their inherent high magnetization, the mesoporous MCNCs pave the way for applying magnetic targeting drug carriers in antitumor therapeutics.

KEYWORDS: mesoporosity · magnetic colloidal nanocrystal clusters · hydrophobic drug delivery · biocompatibility · colloidal stability

Magnetic nanoparticles, especially iron oxides, have been subjected to extensive studies in the past few decades[1,2] owing to their unique magnetic responsiveness and potential in bioseparation[3,4] and drug delivery.[5,6] The ideal magnetic material for bioapplication should possess suitable surface area to maximize loading target objects and avoid any cytotoxic effect, quick magnetic response for fast separation, and excellent biocompatibility.[7−10] Exciting progress has been made in synthesizing iron oxide magnetic nanocrystals with controlled size and shape by thermal decomposition.[11−13] These small magnetic nanocrystals have specific surface area, but the weak magnetic response limits their technical use. Recently, the solvothermal reaction was powerful in directing the formation of submicrometer-sized magnetic colloidal nanocrystal clusters (MCNCs) to improve their magnetic field responsiveness.[14−16] The Li group first described the solvothermal approach to synthesizing MCNCs with high magnetization by reduction of $FeCl_3$ with ethylene glycol.[14] This facile method evokes much interest and is subjected to extensive studies for utilization in physiological conditions. As anticipated, the hydrophilic MCNCs were successfully synthesized by anchoring poly(acrylic acid) (PAA) to the surface of MCNCs as a stabilizer by the Yin group.[15] Along this line, Zhao and co-workers followed the identical route but utilized sodium citrate instead of PAA to improve biocompatibility.[16] Unfortunately, saturation magnetization is improved by the sacrifice of the large surface area. Therefore, finding a facile way to fabricate magnetic particles with high magnetization and suitable surface area seems to be contradictory and difficult to solve.

Paclitaxel (TXL), a hydrophobic anticancer therapeutic drug,[17,18] could effectively treat many tumors, such as non-small cell lung cancers, breast, ovarian, and head carcinomas.[19] The hydrophobic nature of

*Address correspondence to ccwang@fudan.edu.cn.

Received for review November 25, 2010 and accepted January 17, 2011.

Published online February 01, 2011
10.1021/nn103213y

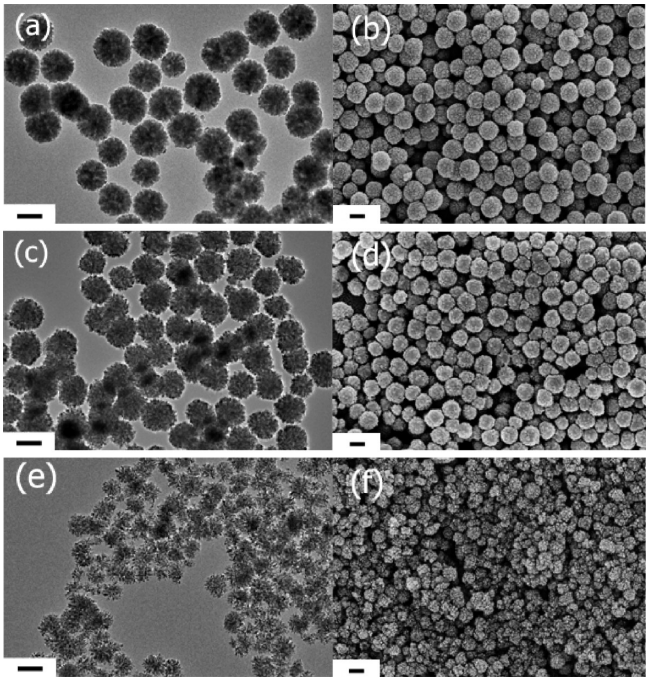

Figure 1. Representative TEM and SEM images of the mesoporous MCNCs synthesized with PGA of (a,b) 0.1, (c,d) 0.5, and (e,f) 1.0 g. All scale bars are 200 nm.

TXL impedes the use of the traditional mode of intravenous administration, thereby limiting its application as an anticancer drug. Recently, novel nanocarriers including magnetic nanoparticles, gold nanoshells, carbon nanotubes, and micelles have been intensively pursued. Usually, magnetic drug nanocarriers comprise magnetic nanoparticulate cores with an organic or inorganic shell, and therapeutic agents are encapsulated within the shell structure.[20,21] Magnetic core/shell nanocarriers can easily be manipulated by an external magnet, which has become known as the "magnetic motor" for site-specific drug delivery applications.[21−23] However, for antitumor drugs with poor water solubility, conjugating the drug onto magnetic nanocarriers often results in inadequate therapeutic efficacy due to the limited loading capacity, weak magnetic response, and poor colloidal stability. Therefore, magnetic nanocarriers, which possess large drug loading capacity, strong magnetic responsiveness, and enhanced colloidal stability, are undoubtedly of significance as versatile carriers for diagnostic and therapeutic applications.

Herein, we report, for the first time, the synthesis of mesoporous MCNCs stabilized by poly(γ-glutamic acid) (PGA) with high magnetization, large surface area, excellent colloidal stability, prominent biocompatibility, and acid degradability, and then we explore their applicability as hydrophobic drug delivery vehicles, which showed high hydrophobic drug loading capacity. Our novel strategy is to manipulate the secondary structures of magnetic colloidal nanocrytals to form mesoporous MCNCs based on our previous work about fabrication of solid and hollow porous MCNCs.[24,25] The obtained mesoporous MCNCs combine the ability to harness the excellent surface area properties of an individual nanocrystal with the knack to utilize the high magnetization of collective properties. PGA-modified mesoporous MCNCs have the advantages of prominent biocompatibility, high water-dispersibility and stability, and robust carboxylate groups that are flexible for further surface modification.[26] More importantly, we found that the PGA could greatly manipulate the secondary structure of magnetic colloidal nanocrystals and flexibly tune both the surface areas and pore sizes, then the very large surface area of mesoporous MCNCs could be prepared under the control of PGA chains. The synthetic procedure is facile and straightforward through a one-pot self-assembly route. TEM and UV−vis results also proved that the mesoporous MCNCs are susceptible to acid etching at lower pH values (4.5−5.5). In light of the strength of such material, we carefully investigate the potential of the prepared mesoporous MCNCs as hydrophobic drug delivery vehicles, using TXL as the model drug. The experimental results demonstrated that the mesoporous MCNCs could load TXL as much as 35.0 wt %, and MTT assay showed the greatly enhanced antitumor efficacy compared with free drug.

RESULTS AND DISCUSSION

Monodisperse high magnetization biocompatible mesoporous MCNCs were synthesized *via* a solvothermal reaction with iron(III) chloride hexahydrate as precursor, ethylene glycol as reducing agent, NH_4OAc

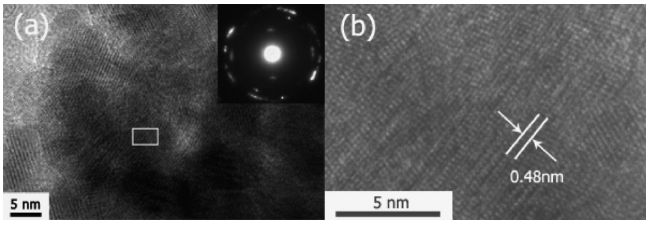

Figure 2. (a) Typical TEM image of mesoporous MCNC synthesized with PGA of 0.5 g and SAED pattern of the cluster (inset). (b) HRTEM image of the boxed region of part a.

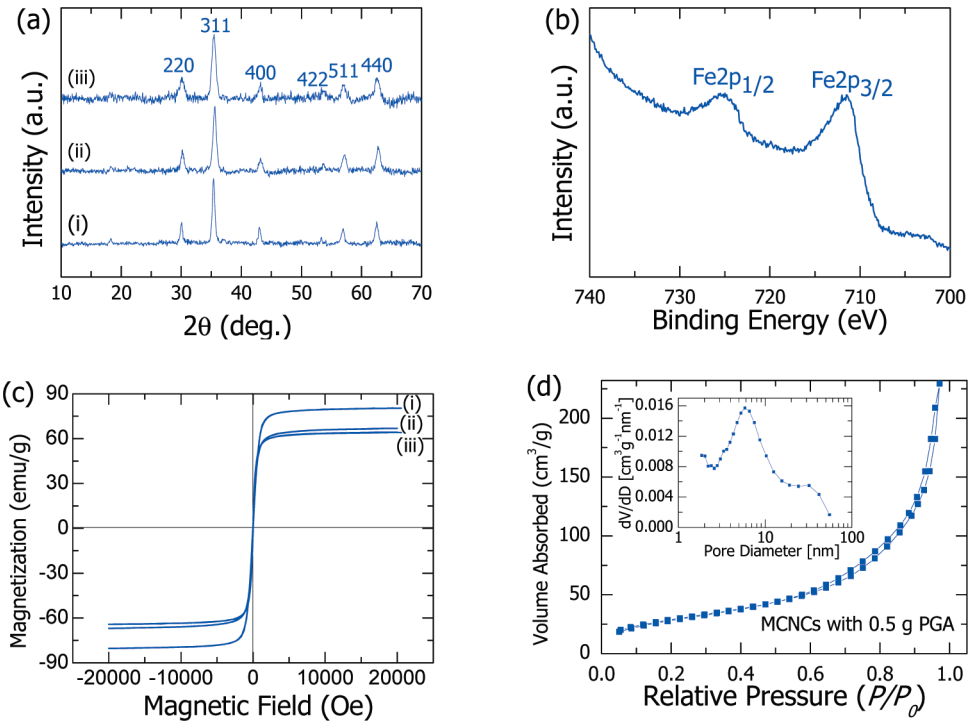

Figure 3. (a) XRD patterns of mesoporous MCNCs obtained with PGA of (i) 0.1, (ii) 0.5, and (iii) 1.0 g. (b) XPS spectrum of mesoporous MCNCs synthesized with PGA of 0.5 g. (c) Magnetic hysteresis curves of mesoporous MCNCs obtained with PGA of (i) 0.1, (ii) 0.5, and (iii) 1.0 g. (d) Nitrogen adsorption−desorption isotherms and pore size distribution (inset) of mesoporous MCNCs synthesized with PGA of 0.5 g.

and biocompatible PGA as electrostatic stabilization agent. As shown in representative transmission electron microscopy (TEM) images in Figure 1a,c, when the initial PGA concentration is increased from 0.1 to 0.5 g, the mesoporous MCNCs spontaneously aggregated by the primary Fe_3O_4 nanocrystals are uniform both in size and in shape and the mesoporous structure becomes more distinct. When the feeding amount of PGA is further increased to 1.0 g, the MCNCs become morphologically rough, irregular, and structurally loose (Figure 1e). The size of the mesoporous MCNCs decreases from 233, 219, to 140 nm with an increase of PGA content from 0.1, 0.5, to 1.0 g, as shown in the representative scanning electron microscopy (SEM) images b, d, and f in Figure 1 and size distribution (Supporting Information, Figure S1).

The secondary structures of mesoporous MCNCs can be observed from a representative isolated cluster obtained with 0.5 g of PGA, and the cluster is composed of small primary building nanocrystals (Figure 2a). Selected area electron diffraction (SAED) pattern taken from individual mesoporous MCNC (inset in Figure 2a) exhibits polycrystalline-like diffraction, confirming that it consists of many magnetite nanocrystals. The high-resolution transmission electron microscopy (HRTEM) image shows that the measured spacing of the crystallographic planes is about 0.48 nm, which agrees well with the distance between the (111) lattice planes of the Fe_3O_4 crystal (Figure 2b).

Figure 3a shows the powder X-ray diffraction (XRD) patterns of the as-prepared mesoporous MCNCs. All of the diffraction peaks can be well indexed to the magnetic cubic structure of Fe_3O_4 (JCPDS 75-1610). The X-ray photoelectron spectrum (XPS) exhibits peaks at 711.7 and 725 eV, which are the characteristic peaks of $Fe2p_{3/2}$ and $Fe2p_{1/2}$ oxidation states, respectively (Figure 3b).[14,16] XRD and XPS confirm that the magnetite mesoporous MCNCs have been successfully

synthesized by this facile and flexible one-pot self-assembly route. Magnetic characterization using a magnetometer at 300 K indicated that the mesoporous MCNCs synthesized with PGA of 0.1, 0.5, and 1.0 g have saturation magnetization values of 80.5 (grain size = 13.7 nm), 66.9 (grain size = 10.4 nm), and 64.4 (grain size = 9.3 nm) emu/g, respectively (Figure 3c). This trend is probably attributed to the higher weight fraction of PGA and small grain sizes in MCNCs with an increase of the PGA feeding amount. Additionally, thermogravimetric (TGA) profiles confirm that PGA is anchored on mesoporous MCNCs so that the weight losses are increased as a function of the feeding PGA (Supporting Information, Figure S2), coherent with the results of saturation magnetization. Nitrogen adsorption−desorption isotherms of MCNCs obtained with 0.5 g of PGA exhibit *I*−*V* type curves, which is characteristic of mesoporosity (Figure 3d). The mesoporous size distribution using the Barrett−Joyner−Halenda (BJH) model shows a peak centered at the mean value of 5.8 nm, indicating that the pores mainly arise from the spaces among the nanocrystallites within a MCNC (inset in Figure 3d). The Brunauer−Emmett−Teller (BET) surface area and total pore volume are calculated to be 106 m^2/g and 0.36 cm^3/g, respectively. The higher BET surface area and larger pore volume strongly support the fact that the product has a mesoporous structure.

To examine the colloid stability of mesoporous samples, 20 mg of MCNCs synthesized with PGA of 0.5 g was dispersed in 80 mL of doubly distilled water by slight sonication, and the suspension could last for more than 48 h, demonstrating their good water-dispersity and stability (Supporting Information, Figure S3). The MCNCs also exhibited excellent colloidal stability in PBS and serum-containing PBS which gives near physiological conditions and justifies further application in biomedicine (Supporting Information, Figure S4). The separation and redispersion behavior of the mesoporous MCNCs was also studied. Under a magnetic field with a permanent magnet (2000 G), the mesoporous MCNCs in their homogeneous dispersion show fast response. All of the mesoporous MCNCs could be attracted the side wall of the vial completely by magnet within 60 s (Supporting Information, Figure S5). Meanwhile, the MCNCs could be redispersed quickly with a slight shake once the magnetic field is removed. All of these experiments suggest that the mesoporous MCNCs possess excellent colloid stability, strong magnetic responsiveness, and redispersibility, which are distinct advantageous to their biomedical applications.

A detailed study of the influence of PGA contents to adjust the mesoporous parameters is presented in Table 1. By increasing PGA from 0.1 to 1.0 g, the specific surface area of MCNCs is improved from 27 to 134 m^2/g and pore volume from 0.11 to 0.57 cm^3/g, correspondingly.

TABLE 1. Porous Characteristics of the MCNCs Synthesized by Varying the Feeding Amount of PGA

feeding amount of PGA (g)	surface area (m^2/g)[a]	pore volume (cm^3/g)	pore size (nm)[b]
0	17	0.03	
0.1	27	0.11	6.2
0.5	106	0.36	5.8
1.0	134	0.57	4.7

[a] Calculated by the BET method. [b] Calculated from the desorption branch of the N_2 isotherm by the BJH model.

Because of the high magnetite (high specific gravity) content in mesoporous MCNCs, we can conclude that the porosity is exceptional enough to be comparable to some of the large surface area and high pore volume of light porous materials. On the other hand, we also noticed that the resulting MCNCs have no porosity when PGA was not utilized in synthesis.

Besides, a series of studies were carried out to understand the formation mechanism of the mesoporous MCNCs. First, a control experiment was conducted without the addition of PGA. In this experiment, close-packed instead of mesoporous MCNCs are observed (Supporting Information, Figures S6 and S7), suggesting the key role of PGA in the formation of mesopores. We further notice that, during the synthesis of PGA-stabilized mesoporous MCNCs, the supernatants isolated from the reaction mediums are indeed emulsions. Due to the limited solubility of PGA used in the study (1000 kDa), we expect that the long PGA chains adopt a globule-like conformation in solvent. As illustrated in Figure 4, the PGA globules stabilize the magnetic nanocrystals (MNCs) formed in the reaction, and meanwhile, NH_3 bubbles evaporated by thermal decomposition of NH_4OAc will allow the PGA globules to reside at the liquid/gas interface to form PGA-stabilized bubbles, which is commonly known as Pickering emulsion.[27,28] As the initial PGA-capped MNs are subjected to self-assembly driven by the system's tendency to minimize the interfacial energies, the PGA-covered NH_3 bubbles are entrapped within the clusters in the process of forming stabilized colloidal clusters. Following the reaction, the trapped NH_3 bubbles in MCNCs are forced out and leave the internal accessible channels for external molecules. In another control experiment, a PGA polymer with much lower molecular weight (20−30 kDa) was used in the synthesis of MCNCs. As the low-molecular-weight PGA polymer is fully soluble in the solution, it is not able to stabilize the Pickering emulsion. As a result, solid MCNCs are obtained in the experiment (Supporting Information, Figures S8 and S9). Similarly, when replacing NH_4OAc with NaOAc to remove bubbles generated in the reaction, only solid MCNCs without mesopores are obtained (Supporting Information, Figures S10 and S11). These experimental results

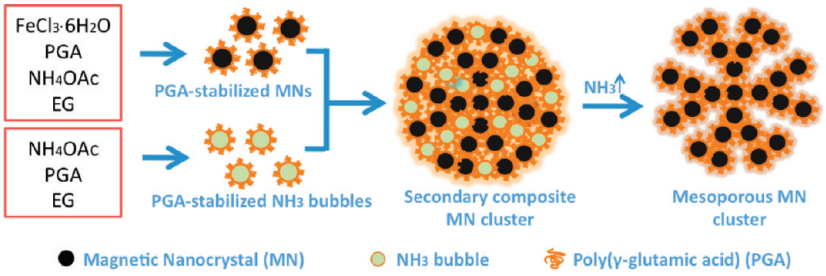

Figure 4. Proposed mechanics of formation of the mesoporous MCNCs.

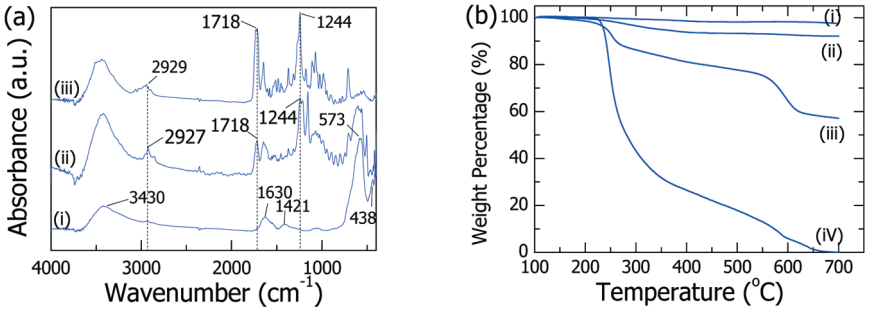

Figure 5. (a) FTIR spectra of (i) mesoporous MCNCs, (ii) TXL-loaded mesoporous MCNCs, and (iii) standard TXL. (b) TG curves of (i) MCNCs synthesized without PGA, (ii) mesoporous MCNCs, (iii) TXL-loaded mesoporous MCNCs, and (iv) standard TXL.

clearly underscored the crucial role of high-molecular-weight PGA and NH_3 bubbles in the formation of mesoporous MCNCs.

The large surface area, high pore volume, and excellent colloidal stability of the as-prepared mesoporous MCNCs drove us to access their potential to be promising drug delivery vehicles for TXL (a fit size of *ca.* 1.8 nm, accessible to the mesopores of MCNCs as shown in Figure S12). TXL was loaded into the mesoporous MCNCs following a modified nanoprecipitation method.[5,6,29] Successful loading of TXL is confirmed by Fourier transform infrared (FTIR) spectra (Figure 5a). The PGA-modified mesoporous MCNCs show peaks at 1630 and 1421 cm^{-1}, indicating the presence of a carboxylate group on the mesoporous MCNCs. The frequencies appearing at 573 and 438 cm^{-1} corresponded to the Fe−O stretching, and a broad band attributed to the O−H vibration is shown at 3430 cm^{-1}. Spectra of standard TXL show characteristic absorption at 1718 and 1244 cm^{-1} ascribed to the symmetric or asymmetric stretch of C═O and C−O, respectively. For mesoporous MCNCs loaded with TXL, the increased absorbance at 1718 cm^{-1} along with the new peak at 1244 cm^{-1} corroborated the incorporation of TXL into the mesoporous MCNCs. Additionally, the strengthened peak at 2927 cm^{-1}, due to the symmetric and asymmetric CH_2 stretching modes, corresponded well with that of TXL. To determine the amount of TXL loaded into the mesoporous MCNCs, TG was employed to directly measure the weight loss of as-prepared product, as shown in Figure 5b. Compared with particles synthesized without PGA, PGA-coated mesoporous MCNCs revealed an approximately 5.4 wt % weight loss ascribed to the amount of PGA immobilized onto the MCNCs. TXL-carrying mesoporous MCNCs revealed an approximately 40.4 wt % weight loss (the drug loading is about 35.0 wt %), indicating that a considerable amount of TXL was loaded into the mesoporous carriers. In curve iii of Figure 5b, the weight loss should correspond to a different process. The first weight loss onset at 253.0 should be the drug on the surface or near the surface of the mesoporous MCNCs, and the second weight loss onset at 594.0 °C should be the drug inside of the pores. It is worth mentioning that, while being incorporated into nanoparticles, hydrophobic agents, such as TXL and camptothecin (CPT), traditionally could not achieve such high loading capacity.[30,31] This result also reflected the potential of the as-prepared mesoporous MCNCs as drug delivery carriers.

The release behavior of TXL-loaded MCNCs was also investigated (Supporting Information, Figure S13). It was observed that only 17.1% of the TXL was released from MCNCs in the 48 h time period at pH 7.4. Compared with refs 25 and 32, the amount of released drug is negligible in such simulated human body fluids, indicating the stability of the drug against physiological environment under protection of mesopores and minimal premature release of drug during the delivery course, which is of great importance for practical drug delivery. Further, it is noteworthy that at lower pH values (4.5−5.5), resembling those in the lysosome, the mesoporous MCNCs are susceptible to acid etching, followed by subsequently disassembled clusters, as shown in the TEM images in Figure 6, and resultant burst release behavior of the entrapped TXL. UV−vis

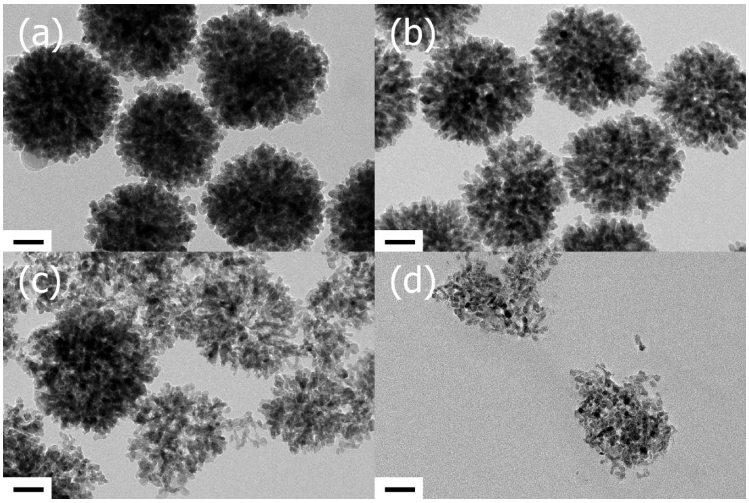

Figure 6. TEM images of mesoporous MCNCs obtained by the "acid-degradable" process in PBS at pH 4.8, 37 °C at (a) 0 h, (b) 24 h, (c) 36 h, and (d) 48 h. All scale bars are 50 nm.

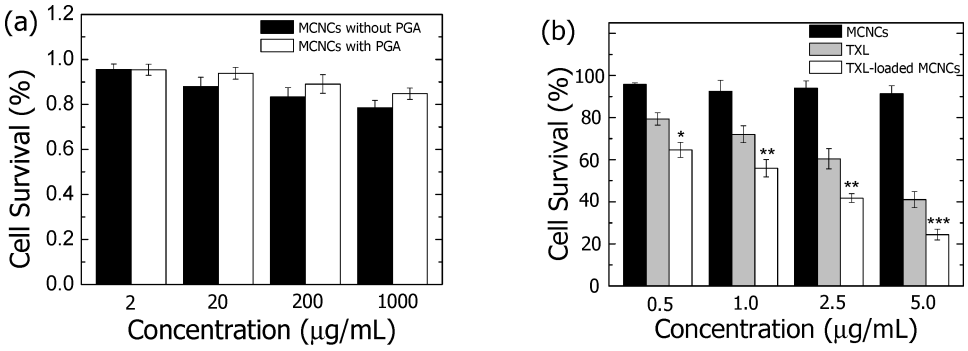

Figure 7. (a) Growth inhibition assay results for HEK 293T cell line with MCNCs with PGA, and MCNCs without PGA after 24 h incubation. Graphs were plotted as particle concentrations of 2, 20, 200, and 1000 μg/mL, respectively. (b) Growth inhibition assay results for HeLa cell line with mesoporous MCNCs, TXL-loaded mesoporous MCNCs, and free TXL after 24 h incubation. Graphs were plotted as TXL concentrations of 0.5, 1.0, 2.5, and 5.0 μg/mL, respectively; $*$ indicates $p < 0.05$, $**$ indicates $p < 0.01$, and $***$ indicates $p < 0.005$, TXL-loaded MCNCs *versus* free TXL. Data represent mean standard deviation of three independent experiments, each performed in triplicate.

was employed to quantify the acid degradation process of as-prepared mesoporous MCNCs (Supporting Information, Figure S14). With the increase of acid degradation time, the intensity of corresponding Fe^{3+} peak of the UV absorption curve is increased. The original colorless solution also gradually became yellow with the prolongation of time, which agreed well with the UV−vis studies. While the representative TEM images give the intuitionistic characterization of the disassembly process of clusters, the UV results quantitatively exhibit the acid degradation process of the mesoporous MCNCs. This is an excellent property for a drug delivery system since the release fashion of the drug was pH-dependent and the carriers could be "degradable", leaving no harm to other normal cells and organs. Combined with their inherent high magnetization, the composited drug can move to a targeting site directly, such as the tumor tissue, and kill cancer cells. Therefore, more detailed investigation and relative animal experiments are underway to further explore the phenomenon and rational design of acid-responsive carriers.

The inhibition of cell growth of non-drug-loaded mesoporous MCNCs, TXL-loaded mesoporous MCNCs, as well as the free TXL was investigated using MTT assay. The data clearly showed that non-drug-loaded mesoporous MCNCs did not show any clear cytotoxicity against normal cells (HEK 293T cells) and revealed the good biocompatibility of PGA-stabilized mesoporous MCNCs, which excelled MCNCs without PGA (Figure 7a). Inconceivably, TXL-carrying mesoporous MCNCs exhibited much higher cytotoxic effect on HeLa cell growth and proliferation than that observed with equivalent doses of TXL in the solution (Figure 7b). We also give statistical information regarding the significance of the results obtained the two-tail p values based on the comparison between the cytotoxicity of TXL-loaded MCNCs and free TXL (Figure 7b), and it could be found that all p values were below 0.05, a statistical boundary, demonstrating the statistical significance of the results. The improvement of inhibitory effect of TXL-loaded mesoporous MCNCs stemmed from the sustained release of the drug molecule out

from the carriers.[6,33] Another point worth noticing was that mesoporous MCNCs with high stability and biocompatibility ensured increased cellular uptake and efficiently released the guest drug molecules to take pharmacological action within the cell compartment, thereby weakening the effect stemming from the poor solubility of the drug.[33,34] Thus, combined with their inherent high magnetization, the PGA-modified mesoporous MCNCs will open up the new avenue in *in vivo* delivery of drugs for the treatment of cancer.

CONCLUSION

In summary, we have demonstrated a flexible and facile method for the synthesis of monodisperse mesoporous MCNCs. The mesoporous MCNCs simultaneously possess high magnetization, narrow size distribution, large surface area, excellent colloidal stability, and prominent biocompatibility. Considerable loading capacity of a hydrophobic anticancer drug and enhanced antitumor efficacy of TXL-loaded mesoporous MCNCs were confirmed by MTT assay. This research has important implications in the fabrication of a new family of mesoporous magnetic clusters for target-specific therapeutic applications. Additionally, we expect that the mesoporous MCNCs may provide great promise for bioseparation and catalysis because of their useful magnetic properties and unique microstructure.

METHODS

General Information. Iron(III) chloride hexahydrate ($FeCl_3 \cdot 6H_2O$), ammonium acetate (NH_4OAc), ethylene glycol (EG), and anhydrous ethanol were purchased from Shanghai Chemical Reagents Company (China) and used as received. Poly(γ-glutamic acid) (PGA) was purchased from Dingshunyin Biotechnology Company (China) and used as received. Paclitaxel (TXL) was purchased from Beijing HuaFeng United Technology CO., Ltd. (China) and used as received. Dulbecco's modified Eagle's medium (DMEM), RPMI-1640, fetal bovine serum (FBS), penicillin G, streptomycin, and trypsinase were obtained from GIBCO BRL (Grand Island, NY). Dimethyl sulfoxide (DMSO) and [3-(4, 5-dimethylthiazol-2-yl)-2,5-diphenyltetrazolium bromide] (MTT) were purchased from Sigma. Deionized water was used in all experiments. TEM images were obtained on an H-600 (Hitachi, Japan) transmission electron microscope at an accelerating voltage of 75 kV. HRTEM images were taken on a JEM-2010 (JEOL, Japan) transmission electron microscope at an accelerating voltage of 200 kV. Samples dispersed at an appropriate concentration were cast onto a carbon-coated copper grid. SEM images were performed using a TS-5136MM (TESCAN, Czech) scanning electron microscope at an accelerating voltage of 20 kV. Samples dispersed at an appropriate concentration were cast onto a glass sheet at room temperature and sputter-coated with gold. XRD patterns were collected on a X'Pert Pro (Panalytical, The Netherlands) diffraction meter with Cu Kα radiation at λ = 0.154 nm operating at 40 kV and 40 mA. XPS data were obtained using an RBD upgraded PHI-5000C (Perkin-Elmer, USA) ESCA system with Mg Kα radiation ($h\nu$ = 1253.6 eV) at 250 W and 14.0 kV with a detection angle at 54°. Nitrogen adsorption–desorption measurements were performed on an ASAP2020 (Micromeritics, USA) accelerated surface area analyzer at 77 K. Before measuring, the samples were degassed in a vacuum at 120 °C for at least 6 h. Magnetic characterization was carried out with a vibrating sample magnetometer on a model 6000 physical property measurement system (Quantum Design, USA) at 300 K. FTIR spectra were recorder on a Magna-550 (Nicolet, USA) spectrometer. The samples were dried and mixed with KBr to be compressed to a plate for measurement. TG analysis data were obtained with a Pyrisis-1 (Perkin-Elmer, USA) thermal analysis system under a flowing nitrogen atmosphere at a heating rate of 20 °C/min from 100 to 700 °C. The size distribution was determined with Image-Pro Plus v4.5 (Media Cybernetics, USA) by measuring 500 clusters based on SEM images.

Synthesis of Mesoporous Magnetic Iron Oxide Colloidal Nanocrystals Clusters. The mesoporous magnetic colloidal nanocrystal clusters (MCNCs) were prepared through a modified solvothermal reaction:[24,25] 1.35 g of 5 mmol $FeCl_3 \cdot 6H_2O$, 3.85 g of 0.05 mol NH_4Ac, and 0.50 g of PGA were dissolved in 70 mL of ethylene glycol. The mixture was stirred vigorously for 1 h at 160 °C under the protection of N_2 to form a homogeneous brownish solution and then transferred into a Teflon-lined stainless-steel autoclave (100 mL capacity). The autoclave was heated to 200 °C and maintained for 16.5 h. Then it was cooled to room temperature. The black MCNCs were then rinsed several times with ethanol under ultrasonic conditions to effectively remove the solvent. The MCNCs were separated from the supernatant by using magnetic force during each rinsing step.

Preparation of TXL-Loaded Mesoporous MCNCs. To incorporate the TXL into the pores of MCNCs, mesoporous MCNCs were well-dispersed in a concentrated solution of TXL, followed by a modified nanoprecipitation method.[5,6,29] Specifically, 10 mg of MCNCs was dispersed in 3 mL of ethanol solution containing 6 mg of TXL by mechanical stirring for 4 h, and then 6 mL of deionized water was added dropwise for 30 min. The resultant mixture was stirred for another 12 h until the solvent was evaporated. The loaded MCNCs were washed repeatedly with PBS (pH 7.4) and deionized water for removal of free TXL, dried under vacuum, and stored in a freezer before characterization and usage.

Cell Culture. A human embryonic kidney cell line, human embryonic kidney (HEK) 293T cells, was cultured in Dulbecco's modified Eagle's medium (DMEM) supplemented with 10% fetal bovine serum (FBS) and 1% antibiotics (100 U/mL penicillin and 0.1 mg/mL streptomycin) at 37 °C in a humidified incubator containing 5% CO_2. Before use of the nanocarriers, they were carefully tiled into a thin layer on a piece of filter paper and exposed to ozone-ultraviolet irradiation for 24 h. For a human cervical carcinoma cell line, HeLa cells were cultured in RPMI-1640 supplemented with 10% fetal bovine serum (FBS) and 1% antibiotics (100 U/mL penicillin and 0.1 mg/mL streptomycin) at 37 °C in 5% CO_2 humid incubator. The cells were subcultured twice weekly.

***In Vitro* Cytotoxicity and Cell viability Study.** The *in vitro* cytotoxicity of PGA-unmodified MCNCs and PGA-modified MCNCs was assessed on HEK 293T cells using the MTT method. Specifically, 100 μL of cells was seeded in a 96-well flat culture plate at a density of 1×10^4 cells per well and were subsequently incubated for 24 h to allow attachment. Then samples with different concentrations (2, 20, 200, 1000 μg/mL) were added to each group (three wells) for 24 h. Twenty microliters of MTT solution (5 mg/mL in PBS) was added to the wells and incubated for 4 h. MTT internalization was terminated by aspiration of the media, and the cells were lysed with 150 μL of DMSO. The absorbance of the suspension was measured at 490 nm on an ELISA reader. Cell viability was calculated by means of the following formula:

$$\text{cell viability } (\%) = \frac{OD_{490(\text{sample})} - OD_{490(\text{blank})}}{OD_{490(\text{control})} - OD_{490(\text{blank})}} \times 100\%$$

The cell viability of MCNCs, TXL-loaded MCNCs, as well as free TXL against HeLa cells was measured by the MTT assay.

The experiment was carried out as an *in viro* cytotoxicity method. Cell viability graphs were plotted as TXL concentration (0.5, 1.0, 2.5, 5.0 μg/mL).

Acknowledgment. We gratefully acknowledge the support of the National Science Foundation of China (Grant Nos. 20974023, 21034003, and 51073040), the National Science Foundation for Distinguished Young Scholars of China (50525310), Shanghai Committee of Science and Technology, China (Grant No. 10XD1400500). We thank Prof. H. Peng at Fudan University for helpful discussions.

Supporting Information Available: Size distribution and TG curves of MCNCs, TEM images and nitrogen adsorption–desorption isotherms of control experiments, schematic representation of the TXL molecule, drug release profile of TXL from mesoporous MCNCs. This material is available free of charge *via* the Internet at http://pubs.acs.org.

REFERENCES AND NOTES

1. Sun, S. H.; Murray, C. B.; Weller, D.; Folks, L.; Moser, A. Monodisperse FePt Nanoparticles and Ferromagnetic FePt Nanocrystal Superlattices. *Science* **2000,** *287*, 1989–1992.
2. Wang, X.; Zhuang, J.; Peng, Q.; Li, Y. D. A General Strategy for Nanocrystal Synthesis. *Nature* **2005,** *437*, 121–124.
3. Deng, Y. H.; Qi, D. W.; Deng, C. H.; Zhang, X. M.; Zhao, D. Y. Superparamagnetic High-Magnetization Microspheres with an Fe_3O_4@SiO_2 Core and Perpendicularly Aligned Mesoporous SiO_2 Shell for Removal of Microcystins. *J. Am. Chem. Soc.* **2008,** *130*, 28–29.
4. Xu, X. Q.; Deng, C. H.; Gao, M. X.; Yu, W. J.; Yang, P. Y.; Zhang, X. M. Synthesis of Magnetic Microspheres with Immobilized Metal Ions for Enrichment and Direct Determination of Phosphopeptides by Matrix-Assisted Laser Desorption Ionization Mass Spectrometry. *Adv. Mater.* **2006,** *18*, 3289–3293.
5. Cheng, K.; Peng, S.; Xu, C. J.; Sun, S. H. Porous Hollow Fe_3O_4 Nanoparticles for Targeted Delivery and Controlled Release of Cisplatin. *J. Am. Chem. Soc.* **2009,** *131*, 10637–10644.
6. Shin, J.; Anisur, R. M.; Ko, M. K.; Im, G. H.; Lee, J. H.; Lee, I. S. Hollow Manganese Oxide Nanoparticles as Multifunctional Agents for Magnetic Resonance Imaging and Drug Delivery. *Angew. Chem., Int. Ed.* **2009,** *48*, 321–324.
7. Lu, A.-H.; Salabas, E. L.; Schuth, F. Magnetic Nanoparticles: Synthesis, Protection, Functionalization, and Application. *Angew. Chem., Int. Ed.* **2007,** *46*, 1222–1244.
8. Jun, Y. W.; Seo, J. W.; Cheon, A. Nanoscaling Laws of Magnetic Nanoparticles and Their Applicabilities in Biomedical Sciences. *Acc. Chem. Res.* **2008,** *41*, 179–189.
9. Gao, J. H.; Gu, H. W.; Xu, B. Multifunctional Magnetic Nanoparticles: Design, Synthesis, and Biomedical Applications. *Acc. Chem. Res.* **2009,** *42*, 1097–1107.
10. Frey, N. A.; Peng, S.; Cheng, K.; Sun, S. H. Magnetic Nanoparticles: Synthesis, Functionalization, and Applications in Bioimaging and Magnetic Energy Storage. *Chem. Soc. Rev.* **2009,** *38*, 2532–2542.
11. Sun, S. H.; Zeng, H. Size-Controlled Synthesis of Magnetite Nanoparticles. *J. Am. Chem. Soc.* **2002,** *124*, 8204–8205.
12. Jana, N. R.; Chen, Y. F.; Peng, X. G. Size- and Shape-Controlled Magnetic (Cr, Mn, Fe, Co, Ni) Oxide Nanocrystals *via* a Simple and General Approach. *Chem. Mater.* **2004,** *16*, 3931–3935.
13. Park, J.; An, K. J.; Hwang, Y. S.; Park, J. G.; Noh, H. J.; Kim, J. Y.; Park, J. H.; Hwang, N. M.; Hyeon, T. Ultra-Large-Scale Syntheses of Monodisperse Nanocrystals. *Nat. Mater.* **2004,** *3*, 891–895.
14. Deng, H.; Li, X. L.; Peng, Q.; Wang, X.; Chen, J. P.; Li, Y. D. Monodisperse Magnetic Single-Crystal Ferrite Microspheres. *Angew. Chem., Int. Ed.* **2005,** *44*, 2782–2785.
15. Ge, J. P.; Hu, Y. X.; Biasini, M.; Beyermann, W. P.; Yin, Y. D. Superparamagnetic Magnetite Colloidal Nanocrystal Cluster. *Angew. Chem., Int. Ed.* **2007,** *46*, 4342–4345.
16. Liu, J.; Sun, Z. K.; Deng, Y. H.; Zou, Y.; Li, C. Y.; Guo, X. H.; Xiong, L. Q.; Gao, Y.; Li, F. Y.; Zhao, D. Y. Highly Water-Dispersible Biocompatible Magnetite Particles with Low Cytotoxicity Stabilized by Citrate Groups. *Angew. Chem., Int. Ed.* **2009,** *48*, 5875–5879.
17. Markman, M.; Mekhail, T. M. Paclitaxel in Cancer Therapy. *Expert Opin. Pharmacother.* **2002,** *3*, 755–766.
18. Skwarczynski, M.; Hayashi, Y.; Kiso, Y. Paclitaxel Prodrugs: Toward Smarter Delivery of Anticancer Agents. *J. Med. Chem.* **2006,** *49*, 7253–7269.
19. Panchagnula, R. Pharmaceutical Aspects of Paclitaxel. *Int. J. Pharm.* **1998,** *172*, 1–15.
20. Chen, L. B.; Zhang, F.; Wang, C. C. Rational Synthesis of Magnetic Thermosensitive Microcontainers as Targeting Drug Carriers. *Small* **2009,** *5*, 621–628.
21. Deng, Y. H.; Wang, C. C.; Shen, X. Z.; Yang, W. L.; Jin, L.; Gao, H.; Fu, S. K. Preparation, Characterization, and Application of Multistimuli-Responsive Microspheres with Fluorescence-Labeled Magnetic Cores and Thermoresponsive Shells. *Chem.—Eur. J.* **2005,** *11*, 6006–6013.
22. Yoon, T.-J.; Kim, J. S.; Kim, B. G.; Yu, K. N.; Cho, M.-H.; Lee, J.-K. Multifunctional Nanoparticles Possessing a "Magnetic Motor Effect" for Drug or Gene Delivery. *Angew. Chem., Int. Ed.* **2005,** *44*, 1068–1071.
23. Kim, J.; Kim, H. S.; Lee, N.; Kim, T.; Kim, H.; Yu, T.; Song, I. C.; Moon, W. K.; Hyeon, T. Multifunctional Uniform Nanoparticles Composed of a Magnetite Nanocrystal Core and a Mesoporous Silica Shell for Magnetic Resonance and Fluorescence Imaging and for Drug Delivery. *Angew. Chem., Int. Ed.* **2008,** *47*, 8438–8441.
24. Luo, B.; Song, X. J.; Zhang, F.; Xia, A.; Yang, W. L.; Hu, J. H.; Wang, C. C. Multi-Functional Thermosensitive Composite Microspheres with High Magnetic Susceptibility Based on Magnetite Colloidal Nanoparticle Clusters. *Langmuir* **2010,** *26*, 1674–1679.
25. Luo, B.; Xu, S.; Ma, W. F.; Wang, W. R.; Wang, S. L.; Guo, J.; Yang, W. L.; Hu, J. H.; Wang, C. C. Fabrication of Magnetite Hollow Porous Nanocrystal Shells as Drug Carrier for Paclitaxel. *J. Mater. Chem.* **2010,** *20*, 7107–7113.
26. Li, C. Poly(L-glutamic acid)-Anticancer Drug Conjugates. *Adv. Drug Delivery Rev.* **2002,** *54*, 695–713.
27. Suzuki, D.; Tsuji, S.; Kawaguchi, H. Janus Microgels Prepared by Surfactant-Free Pickering Emulsion-Based Modification and Their Self-Assembly. *J. Am. Chem. Soc.* **2007,** *129*, 8088–8089.
28. Kim, J.-W.; Fernandez-Nieves, A.; Dan, N.; Utada, A. S.; Marquez, M.; Weitz, D. A. Colloidal Assembly Route for Responsive Colloidosomes with Tunable Permeability. *Nano Lett.* **2007,** *7*, 2876–2880.
29. Dhar, S.; Gu, F. X.; Langer, R.; Farokhzad, O. C.; Lippard, S. J. Targeted Delivery of Cisplatin to Prostate Cancer Cells by Aptamer Functionalized Pt(IV) Prodrug-PLGA–PEG Nanoparticles. *Proc. Natl. Acad. Sci. U.S.A.* **2008,** *105*, 17356–17361.
30. Lu, J.; Liong, M.; Zink, J. I.; Tamanoi, F. Mesoporous Silica Nanoparticles as a Delivery System for Hydrophobic Anticancer Drugs. *Small* **2007,** *3*, 1341–1346.
31. Liong, M.; Lu, J.; Kovochich, M.; Xia, T.; Ruehm, S. G.; Nel, A. E.; Tamanoi, F.; Zink, J. I. Multifunctional Inorganic Nanoparticles for Imaging, Targeting, and Drug Deliver. *ACS Nano* **2008,** *2*, 889–896.
32. Yan, Q.; Yuan, J. Y.; Cai, Z. N.; Xin, Y.; Kang, Y.; Yin, Y. W. Voltage-Responsive Vesicles Based on Orthogonal Assembly of Two Homopolymers. *J. Am. Chem. Soc.* **2010,** *132*, 9268–9270.
33. Jin, C.; Bai, L.; Wu, H.; Song, W. J.; Guo, G. Z.; Dou, K. F. Cytotoxicity of Paclitaxel in Corporated in PLGA Nanoparticles on Hypoxic Human Tumor Cells. *Pharm. Res.* **2009,** *26*, 1776–1784.
34. Kim, J.; Kim, H. S.; Lee, N.; Kim, T.; Kim, H.; Yu, T.; Song, I. C.; Moon, W. K.; Hyeon, T. Multifunctional Uniform Nanoparticles Composed of a Magnetite Nanocrystal Core and a Mesoporous Silica Shell for Magnetic Resonance and Fluorescence Imaging and for Drug Delivery. *Angew. Chem., Int. Ed.* **2008,** *47*, 8438–8441.